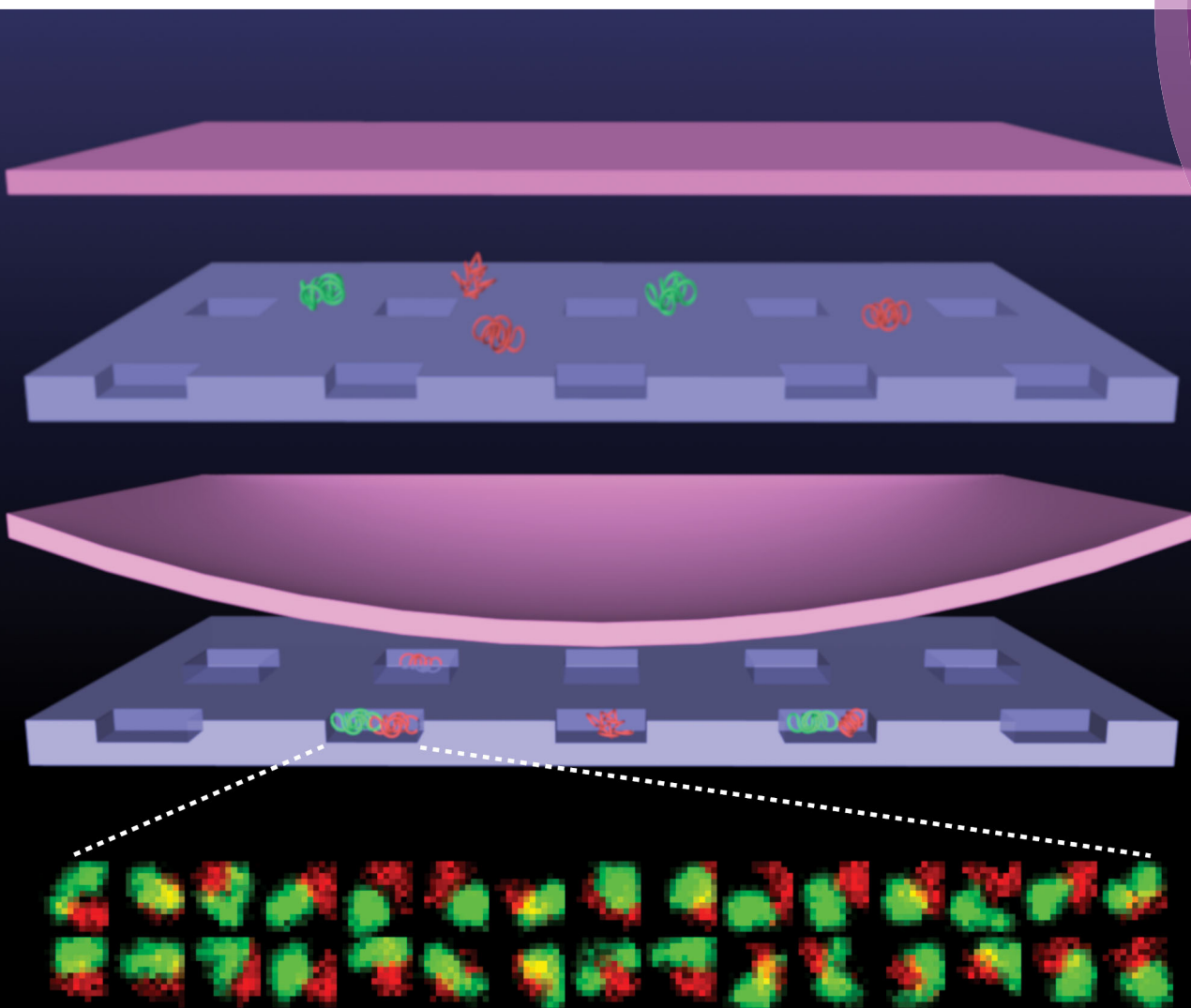


Soft Matter

rsc.li/soft-matter-journal



ISSN 1744-6848



PAPER

Walter Reisner et al.

Probing the organization and dynamics of two DNA chains trapped in a nanofluidic cavity



Cite this: *Soft Matter*, 2018,
14, 8455

Probing the organization and dynamics of two DNA chains trapped in a nanofluidic cavity

Xavier Capaldi, †^a Zezhou Liu, †^a Yuning Zhang, ^a Lili Zeng, ^a Rodrigo Reyes-Lamothe^b and Walter Reisner*^a

Here we present a pneumatically-actuated nanofluidic platform that has the capability of dynamically controlling the confinement environment of macromolecules in solution. Using a principle familiar from classic devices based on soft-lithography, the system uses pneumatic pressure to deflect a thin nitride lid into a nanoslit, confining molecules in an array of cavities embedded in the slit. We use this system to quantify the interactions of multiple confined DNA chains, a key problem in polymer physics with important implications for nanofluidic device performance and DNA partitioning/organization in bacteria and the eukaryotes. In particular, we focus on the problem of two-chain confinement, using differential staining of the chains to independently assess the chain conformation, determine the degree of partitioning/mixing in the cavities and assess coupled diffusion of the chain center-of-mass positions. We find that confinement of more than one chain in the cavity can have a drastic impact on the polymer dynamics and conformation.

Received 13th July 2018,
Accepted 28th August 2018
DOI: 10.1039/c8sm01444b
rsc.li/soft-matter-journal

1 Introduction

When a polymer is confined at a scale below its free solution gyration radius, the equilibrium and dynamic properties of the chain will be altered. Over the past decade nanofluidic technology has emerged that harnesses the power of this nanoconfinement physics to perform parallel manipulations over large numbers of confined chains. Arrays of nanochannels can be used to stretch many DNA molecules in parallel for high-throughput mapping.^{1–3} Embedding nanotopography in a nanoslit, such as nanogroove and nanopit features etched deeper than the surrounding slit, creates local changes in entropy that give rise to a free energy landscape for simultaneous trapping and conformational manipulation of single chains.⁴ For example, ‘digitized’ or ‘tetris’-like conformations are formed when single polymers partition their contour between multiple adjacent nanopits, and nanogrooves extend DNA in the presence of a nanoslit gap permitting additional hydrodynamic access.⁵ These embedded nanotopography devices also serve as powerful experimental models for understanding single-molecule transport in free energy landscapes.^{6–9} Active nanofluidic approaches, such as ‘Convex-lens Induced Confinement,’ can create dynamic confinement variation by effectively adjusting the nanoslit gap *in situ*.¹⁰ Active approaches

create a ‘top-loading’ effect, driving molecular analytes into confined features from above.

Here we use an implementation of top-loading nanofluidics, based on pneumatically actuated nanoscale nitride membranes, to study the conformation, organization and dynamics of two polymer chains confined in a cavity. Remarkably, while small, chemically identical particles will always mix in equilibrium, in confinement, polymers can segregate (*i.e.* demix) as a fundamental consequence of chain interconnectivity and entropy maximization,¹¹ a fundamental problem in polymer physics¹² with key technological and biological implications. For example, the degree to which multiple chains mix or partition in small pores or cavities could impact the performance of polymer manipulation and separation devices (*e.g.* entropic trapping devices for DNA separation,¹³ DNA entropic recoil,¹⁴ and size-exclusion chromatography¹⁵) when, to enhance throughput, these devices are operated at higher concentrations where multiple polymers might be present in the pore structures. On the biological side, entropically driven polymer segregation may play an important role in how dividing prokaryotes segregate their replicating chromosomes between daughter cells.^{11,16} Polymer physics modelling of how multiple chromosomes are organized in the confined environment of the eukaryotic nucleus is a long-standing problem.¹⁷ Over the past five years, there have been intensive theoretical efforts to model the phase-space of polymer mixing/segregation in confined geometries,^{12,16,18–21} yet there has been almost a complete absence of quantitative experiments to characterize the phase-space and corroborate this theoretical work, due to the difficulty of designing appropriate systems for

^a Department of Physics, McGill University, 3600 rue University, Montreal, Quebec H3A 2T8, Canada. E-mail: reisner@physics.mcgill.ca

^b Department of Biology, McGill University, 33649 Sir William Osler, Montreal, Quebec H3G 0B1, Canada

* These authors contributed equally to this work.

isolating multiple chains. Our recent exploration of confined polymer solutions²² took a step in this direction, but this study focused on systems consisting of many confined chains under hydrodynamic forcing (*e.g.* confined solution physics rather than the physics of a small number of interacting chains).

A related but distinct question is the degree to which small molecules can penetrate larger polymer coils in confined systems. In the bulk context, understanding the static phase behavior of polymer–colloid mixtures^{23–25} and how small colloids diffuse in semidilute polymer solutions and melts^{26–29} are major long-standing problems in soft-matter physics. Simulation studies exist specifically addressing the effect of slit confinement on colloid–polymer systems.^{30,31} Understanding how confinement impacts polymer–colloid phase-behavior and dynamics is a problem of considerable technical importance due to the wide-range of applications involving complex fluids in a confined porous structure, such as porous nanomaterials used as self-assembly scaffolds,³² removing pollutants from porous soils and enhanced oil recovery.³³ Yet, likely due to the difficulty of isolating a precisely defined number of polymers and colloids together in small pores, there have been very few experiments investigating pore or cavity-confined polymer–colloid systems.

The behavior of small colloid particles confined with large polymer chains is also of great importance in biology. As one representative example, many bacteria carry plasmids. Plasmids are small circular DNA molecules that carry useful ancillary genes; plasmids must also be segregated during bacterial division.³⁴ Recent studies suggest that plasmids present at high copy number may not be distributed randomly through the bacteria,^{35,36} and in particular may be excluded from certain chromosomal proximal regions and concentrate at the cell poles. There is currently little understanding of this exclusion mechanism; quantitative experimental studies on multiple polymer organization in confined volumes may shed light on the conditions in which polymer molecules of varying size exclude each other or mutually penetrate.

Our device contains nanocavity structures embedded in a nanoslit. Pneumatic pressure is then applied to a 50 nm thick silicon nitride membrane lid, forcing the membrane to deflect downwards into the nanoslit and inducing confinement in the embedded cavities (Fig. 1). This top-loading approach does not require the use of a dedicated piezo-actuated lens pusher, such as the CLIC approach, and is potentially more suitable for large-scale multiplexing. It is similar in principle to the classic dimple machine,³⁷ but is based on direct-bonded hard materials instead of PDMS, using standard fabrication approaches in the DNA nanofluidics field developed for nanochannel and nanopore devices.

In our experiment, two populations of DNA molecules, one population labeled with the uniform stain YOYO-1 (491/509 nm) and the other with YOYO-3 (612/631 nm), are introduced into the nanoslit prior to membrane deflection. The molecules are present at an initial concentration large enough to ensure a high probability of loading two differentially stained molecules in a single cavity after membrane deflection. By design of our cavities, when a single chain is trapped the chain is confined vertically but only

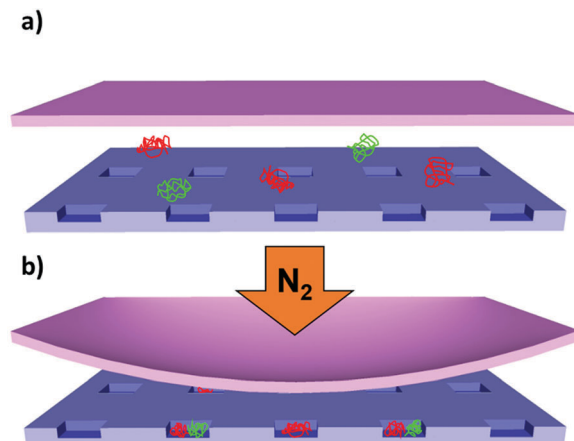


Fig. 1 (a) Schematic demonstrating device operation. The red and green molecules represent differentially-stained λ -DNA which are initially unconfined in the channel environment. (b) Upon the application of nitrogen pressure to deflect the membrane lid downwards, the molecules are trapped inside the embedded features.

weakly confined laterally (for comparison, the gyration radius of λ -DNA is around 0.7 μm ,³⁸ and we expect the vertical cavity depth to be 200 nm when the lid is completely depressed). The vertical confinement leads to a slightly increased gyration radius (0.91 μm ³⁹), so that the molecule has very little room to move in the cavity. This weak lateral confinement does not alter the molecule confirmation but leads to a reduced diffusion (relative to pure slit confinement). When two chains are trapped, however, the effect of the lateral confinement is no longer weak: the conformation and dynamics of the confined chains are very strongly altered due to molecule interaction. Specifically, identical chains with a coil size on the order of the cavity width (48.5 kbp λ -DNA, confined in 2 μm wide, 200 nm deep cavities) undergo clear spatial segregation in the cavities and have a conformation visibly altered by the presence of the second chain. Dynamically, the chains undergo Brownian rotation about the cavity center and have drastically altered diffusional relaxation times. We emphasize that this system is a novel two-polymer confinement state; it cannot exist in bulk or open nanofluidic systems like nanoslits and nanochannels as only a cavity system can enforce long-time interaction of two polymers in a constricted environment. We also explore the behaviour of a small plasmid molecule trapped with a larger coil (6.9 kbp plasmid with λ -DNA in 2 μm wide, 200 nm deep cavities). We find that while the plasmid can diffuse across the λ -DNA coil, the plasmid leads to weaker but still observable interaction effects on the spatial organization of the λ -DNA.

2 Device design and fabrication

We have developed a fabrication process that allows us to couple flexible nanoscale silicon nitride membranes to nanoslits with embedded nano features, enabling a pneumatic top-loading approach that can be coupled to microchannels without requiring a dedicated lens-pusher (Fig. 2a). Our starting substrate is a four-inch borofloat 33 glass wafer (200 μm thick).

Contact UV lithography followed by a $\text{CHF}_3:\text{CF}_4$ etch step is used to create the nanoslit (etched 500 nm deep). Embedded nanocavities, with dimensions of $2 \times 2 \mu\text{m}^2$, are then lithographically defined and etched 200 nm deep with RIE. The etched borofloat substrate is then anodically bonded to a double-side polished silicon/silicon nitride wafer with 50 nm LPCVD nitride (Cornell NanoScale Facility, silicon wafers 400 μm thick). A backside alignment and RIE step is then performed to create the nitride masking layer for a through-wafer KOH etch that leaves a residual nitride membrane over a region of the nanoslit. The loading reservoirs for introducing analyte containing buffer are formed in the same KOH etch. The wafer is cleaved into individual $1 \times 1 \text{ cm}$ devices. A useful feature of this type of device is that the embedded features can be imaged with SEM through the thin nitride lid following device bonding, in principle permitting SEM imaging of channel quality at any time.

In order to perform single molecule imaging in the device and apply pneumatic pressure for DNA transport and membrane deflection, we first mount the device on a dedicated chuck. The chuck, 3D printed with WaterShed XC 11122 plastic (DSM Somos[®]), is interfaced to the device with custom PDMS o-rings that are secured *via* an aluminum retaining ring (Fig. 2b). The polymer constructs are λ -DNA (48.5 kbp, linear topology), stained with YOYO-1, and λ -DNA or pCMV-CLuc 2 Control Plasmid DNA (6.9 kbp), stained with YOYO-3. The staining is performed at a ratio of 10 : 1, bp:fluorophore. The analytes are diluted to $2.5 \mu\text{g mL}^{-1}$ in 10 mMol Tris (8.0 pH) with 2% (vol/vol) beta-mercaptoethanol (BME). The BME is added immediately prior to experiments to reduce the effects of photobleaching and photonicking. Pneumatic pressure, supplied by nitrogen flow interfaced to the loading reservoirs *via* luer connectors, is used to hydrodynamically actuate DNA in the nanoslit. Pneumatic pressure, controlled by Parker VSO-BT Electronic Benchtop pressure

controller run with a custom NI LabVIEW program, is used to deflect the nitride membrane. The pressure controller is calibrated before each use with a manometer. The chuck is mounted on a Nikon Eclipse Ti inverted microscope with a Nikon Plan Apo VC 100 \times oil-immersion objective and an Andor iXon X3 EMCCD camera. Illumination is provided by a metal-halide lamp (Xcite).

Prior to performing an experiment, the device is wetted with running buffer, not containing analytes, and degassed. The reservoir above the flexible membrane lid (isolated from device interior) is also filled with loading buffer to minimize index contrast during imaging. A background image of the nanocavities is captured for both YOYO-1 and YOYO-3 channels. Analyte containing buffer is then introduced in the loading reservoirs and pumped to the nanocavity array. Nitrogen pressure is manually increased to push DNA to the membrane region. Once a large number of molecules have been pumped to the cavity array and are beneath the flexible membrane, the transport pressure is released and the molecules are brought to a halt. We then ramp the membrane pressure to 3 bar over a time range of 10–100 s. If two molecules are trapped in a single cavity, a video is captured. The differentially stained molecules are imaged together by a rotating filter turret which gives a time resolution of 0.84 fps, or a single molecule out of the pair can be imaged in a single channel at 23.49 fps. After recording, the membrane pressure is released and channel pressure is increased to bring fresh unbleached DNA into the field of view. The experimental procedure is then repeated to ensure sufficient statistics.

3 Results and analysis

3.1 Fluorescent microscopy

We capture 10–15 videos containing 100 frames for each DNA population sample. For each video we select only the regions

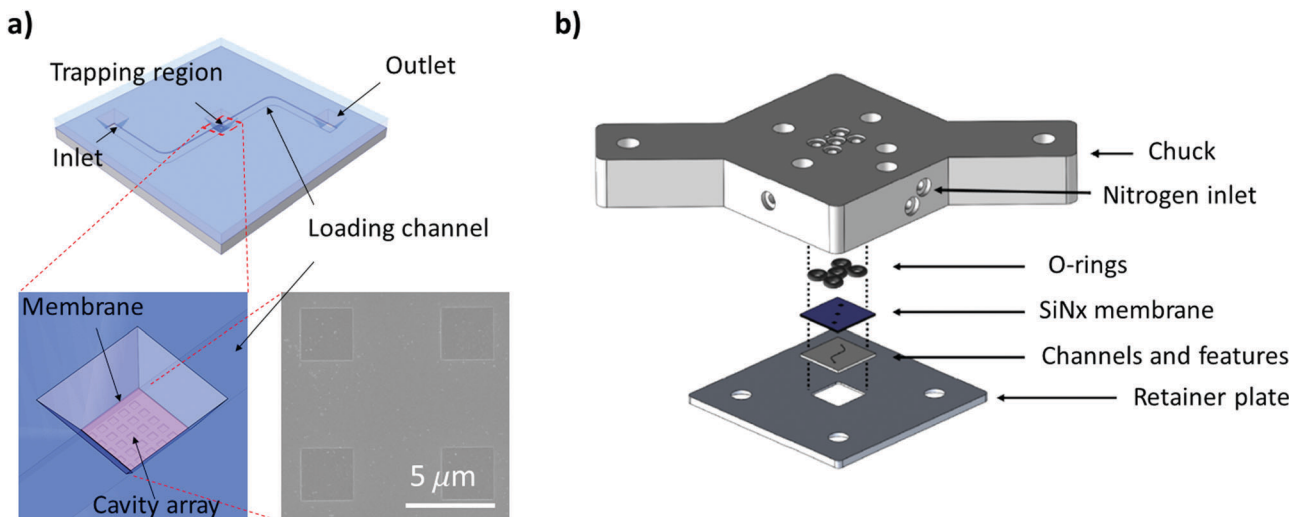


Fig. 2 Design of the fluidic chip and chuck for active pneumatic loading. (a) The trapping region is located at the center of chip, interfaced to a thin nitride membrane (drawn semi-transparent in purple so that cavities underneath can be viewed). An SEM image shows the cavity features etched in the borosilicate glass. Note that this SEM was taken through the 50 nm membrane following device bonding. (b) The 3D-printed chuck used to mount the device for microscopic imaging and interface luer lines for applying nitrogen pressure. Pressure applied to the inlets is used to drive DNA down the loading channel; pressure applied to the central KOH etched reservoir over the trapping region is used to deflect the membrane lid.

corresponding to the cavities where DNA chains are confined. To reduce the influence of the background, we subtract the background intensity (without DNA present) averaged over 100 frames. Fig. 3 shows a time-series of single-molecule (Fig. 3(a and b)) and two-molecule (Fig. 3(c and d)) dynamics in a single cavity. For each DNA population sample we captured 15 videos total from two distinct cavities; the physical behaviour in each cavity was observed to be identical. Comparing Fig. 3(a) and (c), we observe qualitatively that confinement of more than one chain has a strong effect on the molecule

conformation, positioning and dynamics. In the case of single molecule (λ -DNA) confinement, the molecule remains preferentially in the cavity center; in the case of confinement of two molecules of identical size (two λ -DNA's) the molecules segregate and the center of the molecule coils are displaced from the cavity center. The two molecules appear to undergo a Brownian 'rotation' about the cavity center. In contrast to the two λ -DNA molecules, which show clear segregation, the plasmid appears to mix partially with the λ -DNA coil, with some frames indicating overlap of the plasmid and λ -DNA (Fig. 3(d)).

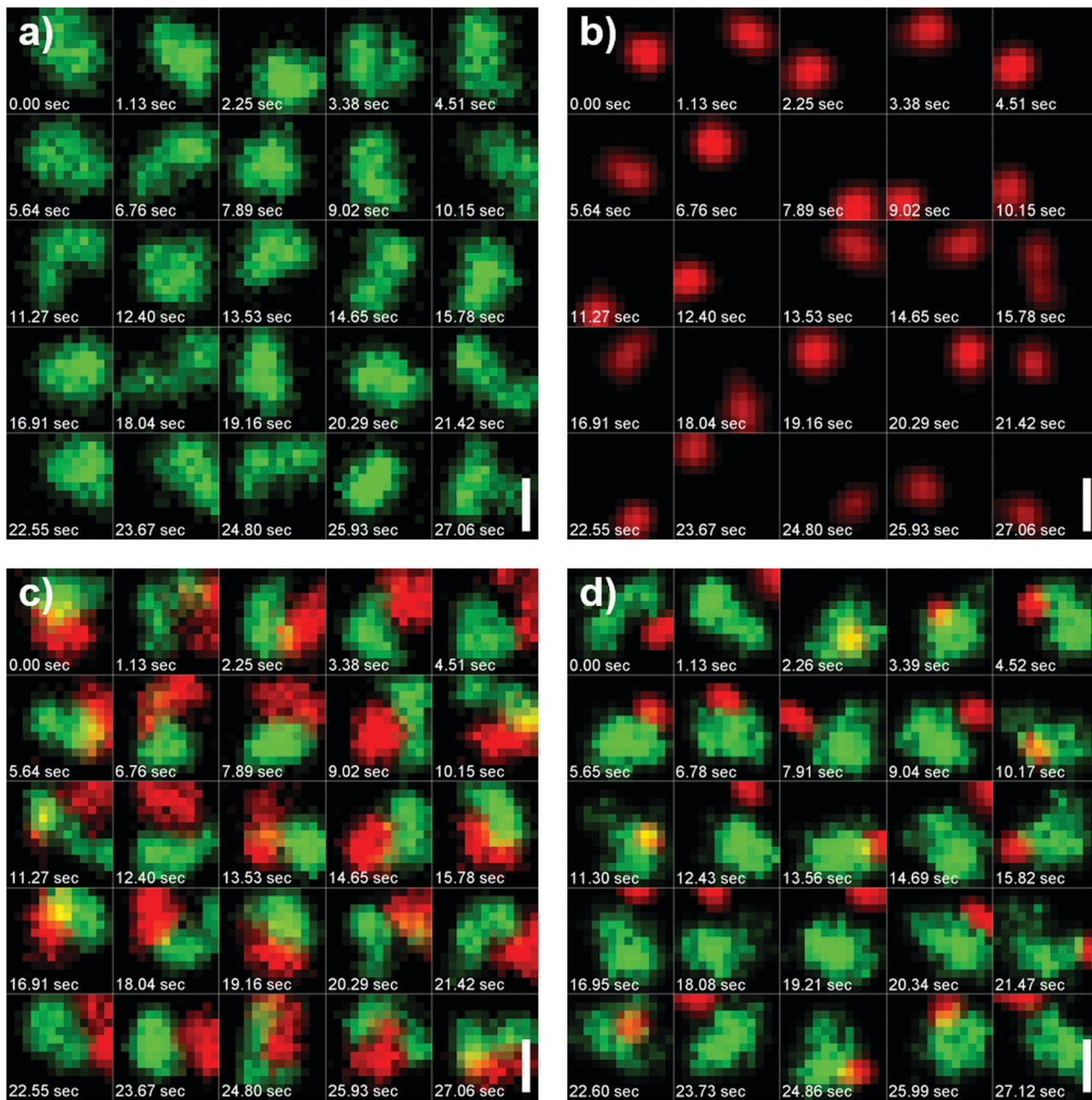


Fig. 3 Fluorescence videomicroscopy frames of cavity confined DNA for cavities with lateral dimension of $2 \times 2 \mu\text{m}$. (a) Single λ -DNA trapped in a cavity. (b) Single plasmid trapped in a cavity (c) two differentially stained λ -DNA molecules in a nanocavity. (d) A λ -DNA (green) and plasmid molecule (red) confined in a cavity. The green color indicates DNA stained with YOYO-1 while the red color indicates DNA stained with YOYO-3. Scale bar is $1 \mu\text{m}$.

3.2 DNA position analysis

In order to quantify the above observations, we perform image analysis to track the center-positions of the cavity confined molecules. The center-position of λ -DNA is obtained by performing a weighted average of position coordinates over the single-molecule fluorescence distribution in the cavity:⁴⁰

$$\mathbf{r}_{CM}(t) = \frac{\int \mathbf{r} \cdot I(\mathbf{r}, t) d^2\mathbf{r}}{\int I(\mathbf{r}, t) d^2\mathbf{r}}. \quad (1)$$

The quantity $\mathbf{r}(t)$ is the position vector; the integral is taken over a ROI that corresponds to the cavity. The quantity $I(\mathbf{r}, t)$

represents the intensity at position \mathbf{r} . To reduce the influence of background fluctuations on the position detection, we apply a Gaussian filter to the image prior to using eqn (1). The plasmid, due to its circular supercoiled topology and smaller size,^{41,42} has a more compact fluorescence distribution that corresponds to a diffraction-limited spot. We find that the plasmid center position can be efficiently tracked using the ImageJ Mosaic Particle Tracking plugin.

Fig. 4(a) shows the distribution of molecule center-positions for a single λ -DNA molecule trapped in a cavity. As the λ -DNA coil and cavity have similar dimensions, chain-wall interactions are quite strong and the λ -DNA is excluded from the cavity

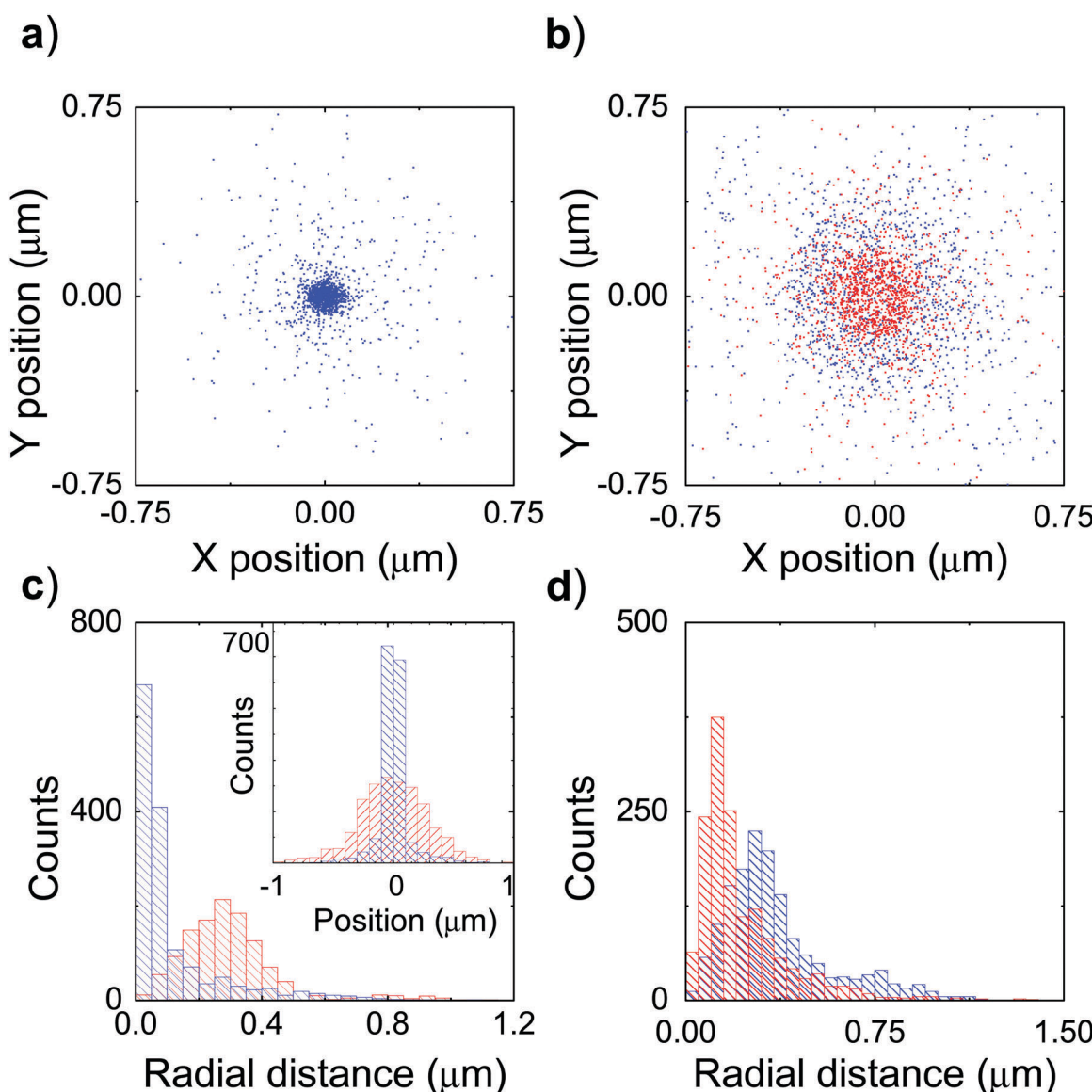


Fig. 4 Center position analysis for λ -DNA. (a) Position distribution for a single λ -DNA molecule. (b) Position distribution for two λ -DNA molecules. Blue squares indicate YOYO-1 stained chain; red squares indicate YOYO-3 stained chain. (c) Radial distance histogram of λ -DNA chain. Blue shaded columns indicate distribution of single λ -DNA molecule. Red shaded columns indicate distribution of λ -DNA molecule while the second λ -DNA is present. The inset shows the horizontal projection of the distribution along the cavity width. (d) Histogram of radial distance for λ -DNA in presence of second λ -DNA. Red shaded columns indicate YOYO-3 stained chains; blue shaded columns indicate YOYO-1 stained chains.

corners and periphery, giving rise to a center-position distribution tightly localized in the cavity middle. Fig. 5(a) shows the position distribution for a single plasmid. As the plasmid has a much smaller gyration radius than the λ -DNA, the excluded region is smaller, and the plasmid can explore a greater portion of the cavity. In fact, we observe that the distribution is spatially uniform and follows the square cavity shape.

Fig. 4(b) shows the position distribution of two λ -DNA molecules. When the second chain is present, due to excluded volume interactions between the coils, the center-position of the chains are forced to explore a greater portion of the cavity, creating a broader position distribution (see Fig. 4(c)). In addition,

we find that the center position distribution for the YOYO-3 labeled chain is slightly more concentrated in the cavity center than the distribution for the YOYO-1 labeled chain (see Fig. 4(d)). This effect might arise from how the different stains alter the chain contour, stiffness and self-interactions. YOYO-1, for example, increases the contour length of DNA⁴³ and there are likely differences in intercalated length between the two stains. A molecule confined in a cavity will have its coil sized fixed by the cavity confinement, but a longer contour length will decrease the chain's entropic elasticity. Possibly, when the stains alter the contour length differentially, the slightly longer and more easily deformed chain is pushed to the cavity periphery as the chain

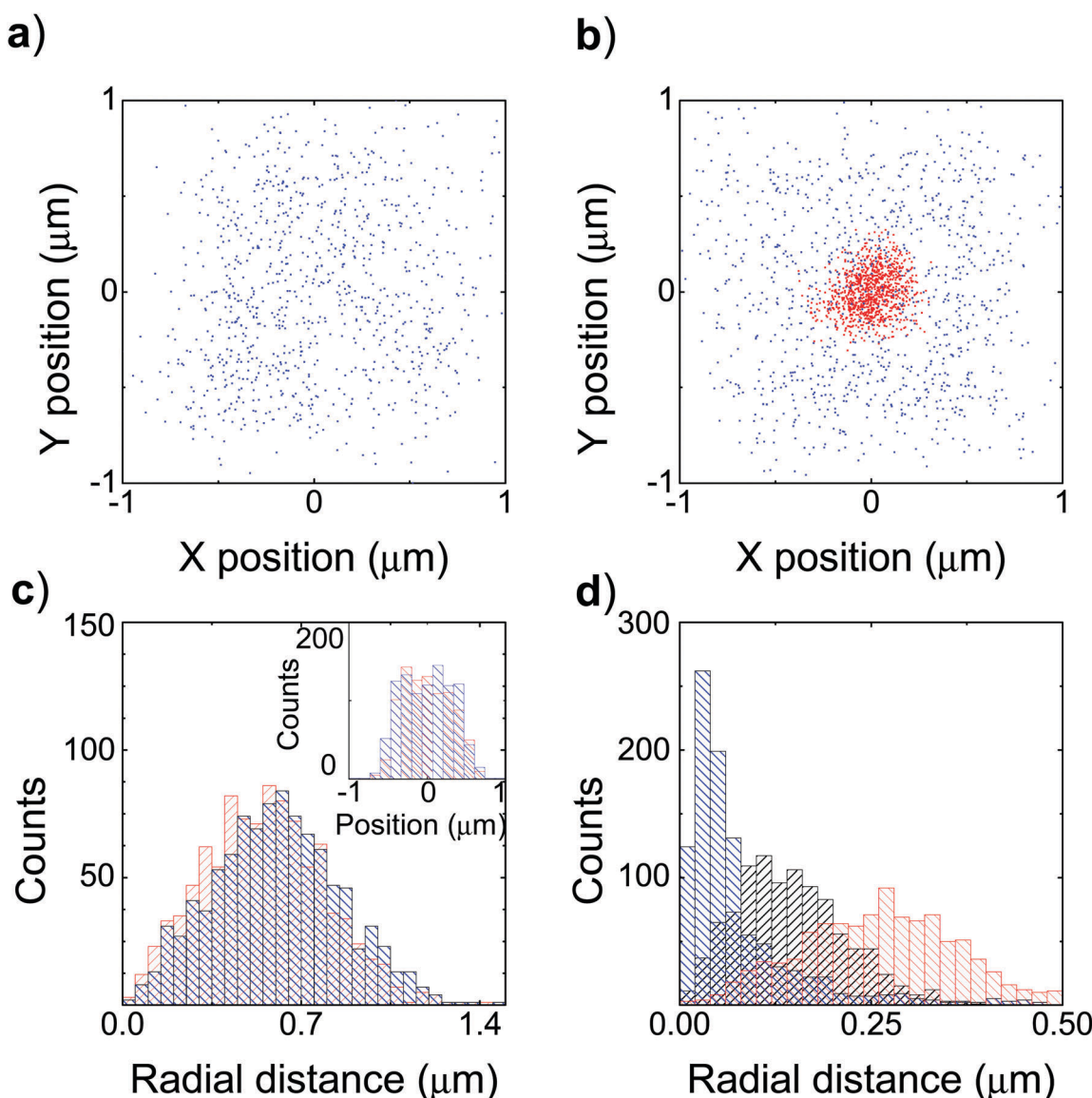


Fig. 5 Center position analysis for plasmid DNA. (a) Position distribution for a single plasmid trapped in the cavity. (b) Position distribution for a plasmid trapped with λ -DNA in the cavity. Blue squares show plasmid positions; red squares show λ -DNA positions. (c) Radial position distribution of plasmid. The blue shaded columns show the distribution for single plasmid; red columns show the plasmid distribution when a λ -DNA is also present. The inset shows for the same quantities the horizontal projection of the distribution along the cavity width. (d) Histogram of radial distance of λ -DNA. The blue shaded columns indicate the distance distribution for single λ -DNA trapping. Black shaded columns indicate the distribution of λ when the plasmid is also present. The red shaded columns indicate the distribution when two λ -DNA molecules are trapped.

closer to the periphery is required to deform more to adopt a greater circumferential extent and conform to the square cavity geometry.

Fig. 5(b) shows the position distribution of λ -DNA and the plasmid when they are trapped together. We observe that the position distribution of the plasmid DNA is not altered by the presence of λ -DNA (Fig. 5(c)), but that the position distribution of λ -DNA is less concentrated in the cavity center (Fig. 5(d)). The plasmid, with its superoiled circular topology, will have a compact anisotropic structure and act very crudely speaking like an elongated pancake.^{41,42} This structure, once aligned with the cavity surfaces, might penetrate the λ -DNA structure relatively easily by passing through the depletion region of lowered DNA concentration near the cavity walls.⁴⁴ This effect, which is consistent with Fig. 3(d), would then explain why the 2D plasmid position distribution is not altered by the λ -DNA. We argue that the shifting of the λ -DNA position distribution might be explained by a depletion interaction induced by the plasmid,⁴⁵ by getting closer to the cavity edges, the λ -DNA frees up more volume for the plasmid conferring greater translational entropy.

3.3 DNA diffusion analysis for single chain trapping

The dynamics of a single DNA molecule confined within a cavity can be modeled as the free Brownian diffusion of a particle within an infinite square well potential.⁴⁶ The molecule's mean-square displacement along x given by:

$$\text{MSD}(\delta t) = \frac{1}{T} \int_0^T [x(t + \delta t) - x(t)]^2 dt \quad (2)$$

Since our device is symmetric in the x and y directions, with the coordinate system aligned with the cavity dimensions, the mean square displacement is the same along the x and y axis and we average results obtained for x and y . The mean-square displacement can be obtained by solving the diffusion equation for a particle in a square box, leading to:

$$\text{MSD}(\delta t) = \frac{L^2}{6} - \frac{16L^2}{\pi^4} \sum_{n=1,3,5,\dots}^{\infty} \frac{1}{n^4} \exp\left[-D\left(\frac{n\pi}{L}\right)^2 \delta t\right] \quad (3)$$

where L is the box width.⁴⁶ As the molecules have a finite size, a zone of excluded-volume will exist about the cavity boundary and the L values extracted will be smaller than the true lateral cavity dimensions. We show the experimental MSD with theoretical fit according to eqn (3) in Fig. 6. Both the diffusion constant D and box width L are fitted.

The DNA diffusion constants obtained are $D_\lambda = 0.055 \pm 0.003 \mu\text{m}^2 \text{s}^{-1}$ (for λ -DNA) and $D_p = 0.68 \pm 0.02 \mu\text{m}^2 \text{s}^{-1}$ (for plasmid). In bulk, $D_{\text{bulk},\lambda} = 0.47 \pm 0.03 \mu\text{m}^2 \text{s}^{-1}$ ⁴⁷ and in a 200 nm nanoslit $D_{\text{slit},\lambda} = 0.1 \mu\text{m}^2 \text{s}^{-1}$,^{48,49} so that cavity confinement creates a two-fold reduction with respect to the slit and a factor of ten with respect to bulk. For a 6.5 kbp plasmid the bulk diffusion constant $D_{\text{bulk},p} = 2.89 \mu\text{m}^2 \text{s}^{-1}$,⁵⁰ cavity confinement thus leads to a 4-fold reduction with respect to bulk. The extracted confinement dimension L of λ -DNA is $0.13 \pm 0.002 \mu\text{m}$ while the confinement dimension of the

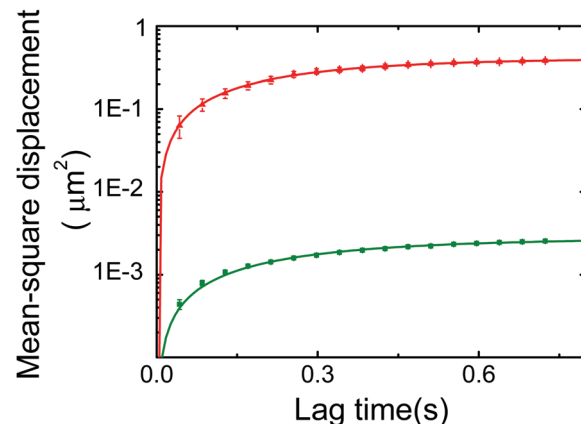


Fig. 6 Mean-square displacement for single λ -DNA trapping (green triangles) and single plasmid trapping (red squares). The solid curve is the fitted diffusion model.

plasmid is $1.57 \pm 0.01 \mu\text{m}$. The radius of gyration for λ -DNA confined in a 200 nm slit is: $r_{g,\lambda} = 0.91 \mu\text{m}$.³⁹ Using $2r_g$ as an estimate of the molecule coil extent, we estimate that the confinement dimension $L \approx d - 2r_g$ where $d = 2 \mu\text{m}$ is the cavity width. The resulting small value $L_\lambda \approx 0.2 \mu\text{m}$ is quite comparable to our measurement, reflecting a scenario where the molecule's center-of-mass position is tightly confined (*i.e.* the molecule has very little room to move before bumping into a cavity side-wall). To estimate the spatial extent of the plasmid, we use measurements for the ColE₁ plasmid, which is of comparable size (6.65 kbp). Voordouw *et al.*⁵⁰ report that for ColE₁ light scattering measurements give $r_g^p = 104 \text{ nm}$, so that $L_p \approx 1.79 \mu\text{m}$. This is the right magnitude but larger than the L_p value we measure, a difference which might arise from plasmid anisotropy and our lower ionic strength.

3.4 Position auto-correlation calculation

We investigate the position auto-correlation of the λ -DNA and plasmid molecule for both single molecule and two-molecule trapping (see Fig. 7). The position auto-correlation function is defined as:

$$C_{\text{auto}}(\delta t) = \langle x(t + \delta t)x(t) \rangle_t \quad (4)$$

where x represents position along either the x - or y -direction with the origin located at the cavity center. The angle bracket indicates a time-average, corresponding to averaging over the entire video length; δt is the correlation lag time. Considering the square symmetry of the cavity, we average the position auto-correlations for the x - and y -directions.

Fig. 7(a and b) shows the autocorrelation functions for single and two-particle trapping; these are well-described by a single exponential function. We define the decorrelation time as the time needed for the correlation function to decay to e^{-1} of its maximum value. The decorrelation time for λ -DNA trapped in a cavity, if no other molecules are present, is $0.25 \pm 0.01 \text{ s}$; the decorrelation time for λ -DNA, trapped in the presence of a plasmid, is $0.29 \pm 0.01 \text{ s}$ and the decorrelation time for λ DNA trapped in the presence of a second λ -DNA molecule is $2.00 \pm 0.1 \text{ s}$.

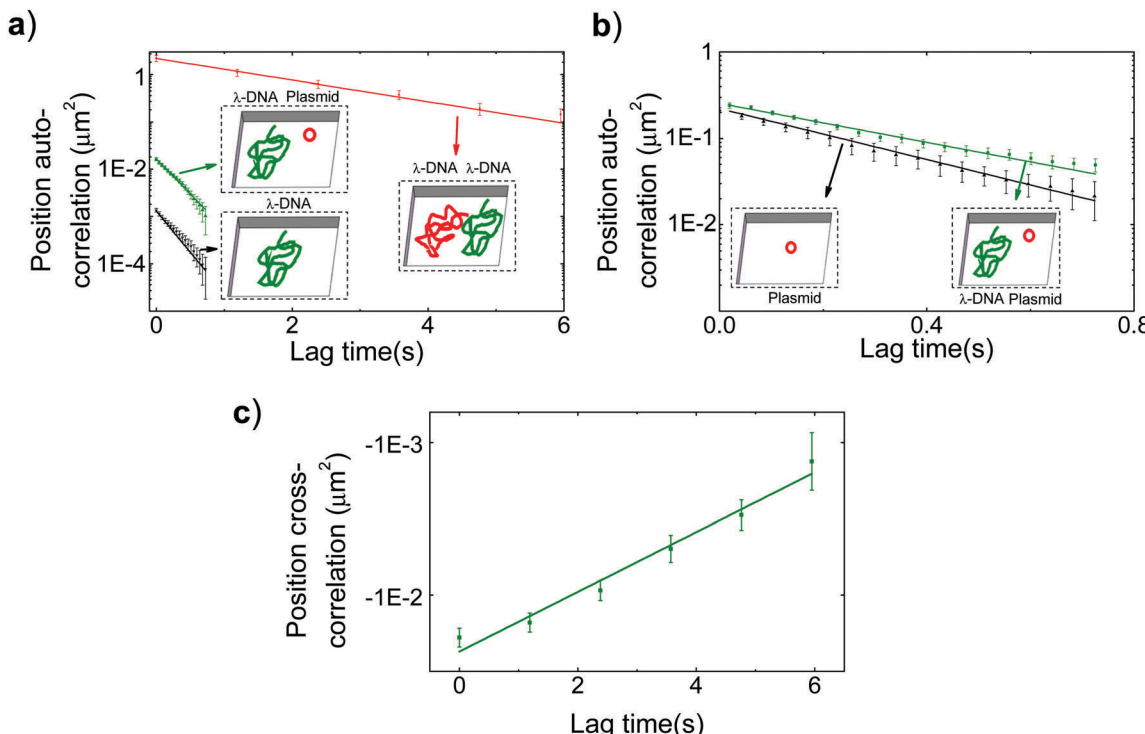


Fig. 7 Position auto-correlation as a function of lag time on a log-linear scale with an exponential fit. (a) Position auto-correlation function for λ -DNA. Red squares indicate the correlation function measured for a λ -DNA molecule trapped in a cavity when there is a second λ -DNA molecule trapped in the same cavity. Green upper triangles indicate the correlation function obtained for λ -DNA when there is a plasmid molecule also trapped in the cavity with the λ -DNA. Black lower triangles indicate the correlation function measured for a λ -DNA molecule trapped in a cavity when there are no other molecules present. (b) Auto-correlation function for plasmid DNA. Green squares indicate the position correlation function of the plasmid in the presence of a λ -DNA molecule trapped in the same cavity as the plasmid. Black upper triangles indicate the position autocorrelation function for the plasmid with no other molecules present. (c) Position cross correlation for trapping of a YOYO-1 stained λ -DNA and a YOYO-3 stained λ -DNA. Exponential fits are shown as bold curves in the same color as the data points. Error bars correspond to standard error arising from measurements over an ensemble of 10 different molecules undergoing equivalent dynamics.

The decorrelation time clearly increases with the presence of additional molecules, and in the case of λ -DNA increases by almost an order of magnitude. The decorrelation time for a plasmid, if no other molecule is trapped, is 0.31 ± 0.01 s; in the presence of a λ -DNA molecule the decorrelation time is 0.39 ± 0.01 s. Qualitatively, we believe that the increasing decorrelation times for two-molecule trapping arise as the second molecule transiently confines the first molecule creating a caging effect. Caging leads to a lower effective diffusion constant for the molecules that then increases the overall decorrelation time.

We also investigate the position cross-correlation between the YOYO-1 stained λ -DNA chain and the YOYO-3 stained λ -DNA chain (Fig. 7(c)). The cross-correlation is defined as

$$C_{\text{cross}}(\delta t) = \langle x_{\text{yo-yo-1}}(t + \delta t)x_{\text{yo-yo-3}}(t) \rangle_t \quad (5)$$

where $x_{\text{yo-yo-1}}$ and $x_{\text{yo-yo-3}}$ represent respectively the position of the YOYO-1 stained chain and the YOYO-3 stained chain at time t along the x - or y -direction. Again, we average the cross-correlation function over x and y directions. The cross-correlation function is negative, indicating anti-correlation arising from the strong segregation between the molecules. The decorrelation time of the cross-correlation is 2.8 ± 0.3 s, comparable in order of magnitude to the autocorrelation decay

time; we hypothesize it is longer than the autocorrelation decay time as the cross-correlation function decorrelates over the time-scale required for both chains to lose their initial joint conformation.

4 Intensity cross-correlation function

As a final measure of the two-chain dynamics, for the case of two λ -DNA molecules we investigate the cross-correlation of the intensity across the cavity. In particular, we compute the intensity cross-correlation function $\langle \delta I_{\text{yo-yo-1}}(x,y,t)\delta I_{\text{yo-yo-3}}(x,y,t + \delta) \rangle$, where δI gives the fluctuation away from the average intensity at position (x,y) inside the cavity. Fig. 8(a–c) shows the intensity cross-correlation for three different times. We find that there is a strong anti-correlated annular well for short times, consistent with the organized rotation of the segregated conformations observed in Fig. 3c. The ‘hill’ of slightly reduced anti-correlation in the cavity center corresponds to configurations where the molecules have drifted to the center and partially mixed, leading to a slight breaking of the organized rotational dynamics and a reduction in anti-correlation. We also compute the cross-correlation function averaged over the entire cavity region (Fig. 8(d)). The averaged cross-correlation

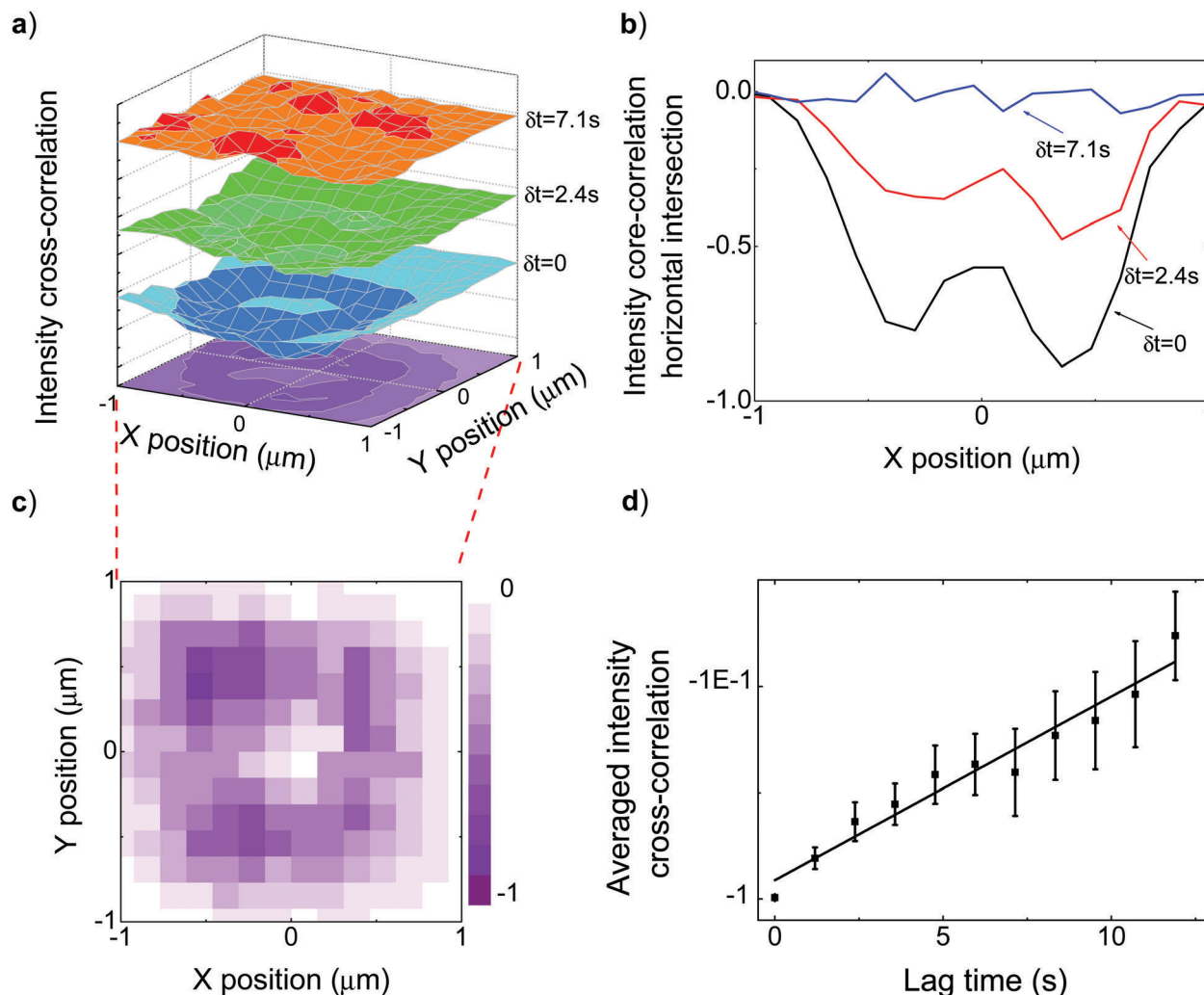


Fig. 8 Intensity cross-correlation function. (a) Surface plot for normalized intensity cross-correlation for different lag times. Orange surface represents cross-correlation function at $\delta t = 7.1$ s, green surface represents cross-correlation function at $\delta t = 2.4$ s and blue surface represents cross-correlation function at $\delta t = 0$. (b) Intensity cross-correlation function from (a) taken along a slice along the x-axis for $y = 0$. (c) Intensity cross-correlation for $\delta t = 0$. (d) Intensity cross-correlation function averaged across cavity versus lag time. The correlation function is fitted with an exponential function that is shown as a black solid curve.

is described well by a single exponential decay and has a decorrelation time of 4.2 ± 0.4 s. This value is comparable in magnitude but slightly larger than the position cross-correlation decay time. We speculate that the position cross-correlation decay time is lower because of the greater confinement of the molecule center positions relative to a particular individual segment or portion of the molecule. The greater confinement of the molecule centers implies that the center positions have to migrate over a smaller distance to swap positions compared with the distance an individual segment needs to traverse to return to a particular location of the cavity.

5 Discussion and conclusion

We have developed a device based on pneumatically actuated flexible membrane lids to capture single and multiple DNA

molecules in a cavity. We find that the molecular organization and dynamics is strongly affected by whether more than one molecule is captured. A single λ -DNA molecule has coil extent on the order of the cavity width. When two molecules are confined together, they exist in a highly partitioned state and appear to undergo a Brownian rotation about the cavity center. We find that even the presence of a small plasmid molecule can alter the λ -DNA state, tending to pull it away from the cavity center. Confinement of more than one molecule has additional non-trivial effects on dynamics, tending to increase overall relaxation times for confined molecular diffusion.

Our system and observations raise some intriguing questions. For example, how might the properties of the organized multiple molecule states vary as a function of the molecule size ratio, molecule number and cavity geometry? Might distinct dynamical regimes exist for two, three or multiple molecule states as a function of cavity dimensions and size ratio? How does varying

the vertical dimension affect molecule partitioning? (Does chain mixing occur as bulk conditions are approached?) Another potential experiment is to only lower the lid partially, so that escape from our traps is possible upon application of a sufficient driving force to overcome the free energy differential. Our system would then enable exploration of how the presence of multiple chains affect escape kinetics. In addition, while the cavities used here are not designed to mimic specific biological systems, our approach can be used to construct cavities close in dimension to bacteria and eukaryotic nuclei. Using extracted *E. coli* genomes⁵¹ to model native Mbp scale DNA representative of bacterial genomes and (crudely) chromosomes of lower eukaryotic cells, we can then create experimental models isolating the effects of confinement from other sources of biological complexity.

We can already compare our experimental results on partitioning/mixing to a proposed phase-diagram deduced for self-avoiding chains by S. Jun *et al.*¹⁶ S. Jun *et al.* uses polymer scaling arguments to predict a phase-space for chain segregation/mixing that depends only on polymer concentration and confinement. Polymer concentration is measured by the ratio r_F/ζ , where r_F is the Flory radius and ζ is the chain correlation length; confinement is measured by r_F/D where D is the dimension of imposed confinement. For the λ -DNA, estimating the Flory radius by the chain gyration radius (0.7 μm), taking D to be the cavity depth (200 nm) and estimating ζ as the coil extent (0.91 μm), we find that $r_F/D = 3.5$ and $r_F/\zeta = 0.77$, which lies in a region of space corresponding to segregation. For the plasmid, following the argument used in S. Jun *et al.*, we take r_F to be 104 nm (plasmid coil size) and let ζ correspond to the correlation length of the much larger molecule (λ -DNA), leading to $r_F/D = 0.52$ and $r_F/\zeta = 0.11$, which lies in the region of the space where mixing is predicted. So, while we do not see evidence of segregation of plasmids and λ -DNA, this is consistent with the theoretical prediction for self-avoiding chains. Possibly plasmid exclusion requires higher chain concentration, more complex chain topology (e.g. supercoiling¹⁶) and/or presence of chain condensing agents, like molecular crowders.^{52,53} We plan to explore these effects in future experiments, using extracted *E. coli* genomes.

Our observation, however, that the presence of a single small compact molecule can impact the behaviour of a larger coil in confinement is unexpected and intriguing. For example, might we detect differences between linearized and circular form plasmids? How does this effect scale with plasmid size and plasmid number? In addition, we show that subtle differences due to chemical stains (e.g. YOYO-1 *versus* YOYO-3) can be detected *via* two-molecule measurements of the chain position distributions. Possibly, this effect could extend to other types of molecular labeling or protein-interactions. Overall, our results suggest that measurements of the physical interactions of multiple confined macromolecules might convey information beyond that of a purely single molecule experiment. From a theoretical point of view, Monte Carlo and Brownian dynamics simulations of multiple chain confinement might clarify the underlying mechanisms responsible for these observations.

Conflicts of interest

There are no conflicts to declare.

Acknowledgements

This work was funded through the Natural Sciences and Engineering Research Council of Canada (NSERC) Discovery Grants Program (Grant No. RGPIN 386212) and the Fonds de recherche du Québec Nature et technologies (FQRNT) Projet d'équipe (PR-180418).

References

- W. Reisner, J. N. Pedersen and R. H. Austin, *Rep. Prog. Phys.*, 2012, **75**, 106601.
- W. Reisner, K. J. Morton, R. Riehn, Y. M. Wang, Z. Yu, M. Rosen, J. C. Sturm, S. Y. Chou, E. Frey and R. H. Austin, *Phys. Rev. Lett.*, 2005, **94**, 196101.
- J. Mannion, C. Reccius, J. Cross and H. Craighead, *Biophys. J.*, 2006, **90**, 4538–4545.
- A. R. Klotz, L. Duong, M. Mamaev, H. W. de Haan, J. Z. Y. Chen and W. W. Reisner, *Macromolecules*, 2015, **48**, 5028–5033.
- W. Reisner, N. B. Larsen, A. Silahtaroglu, A. Kristensen, N. Tommerup, J. O. Tegenfeldt and H. Flyvbjerg, *Proc. Natl. Acad. Sci. U. S. A.*, 2010, **107**, 13294–13299.
- M. B. Mikkelsen, W. Reisner, H. Flyvbjerg and A. Kristensen, *Nano Lett.*, 2011, **11**, 1598–1602.
- C. L. Vestergaard, M. B. Mikkelsen, W. Reisner, A. Kristensen and H. Flyvbjerg, *Nat. Commun.*, 2016, **7**, 10227.
- J. T. D. Bonis-O'Donnell, W. Reisner and D. Stein, *New J. Phys.*, 2009, **11**, 075032.
- D. Kim, C. Bowman, J. T. D. Bonis-O'Donnell, A. Matzavinos and D. Stein, *Phys. Rev. Lett.*, 2017, **118**, 048002.
- D. J. Berard, F. Michaud, S. Mahshid, M. J. Ahamed, C. M. J. McFaul, J. S. Leith, P. Bérubé, R. Sladek, W. Reisner and S. R. Leslie, *Proc. Natl. Acad. Sci. U. S. A.*, 2014, **111**, 13295–13300.
- S. Jun and A. Wright, *Nat. Rev. Microbiol.*, 2010, **8**, 600–607.
- Y. Jung, J. Kim, S. Jun and B.-Y. Ha, *Macromolecules*, 2012, **45**, 3256–3262.
- J. Han, *Science*, 2000, **288**, 1026–1029.
- S. W. P. Turner, M. Cabodi and H. G. Craighead, *Phys. Rev. Lett.*, 2002, **88**, 128103.
- I. Teraoka, *Polymer Solutions*, John Wiley & Sons, Inc., 2002.
- S. Jun and A. Wright, *Nat. Mater.*, 2010, **8**, 600–607.
- M. Barbieri, A. Scialdone, A. Gamba, A. Pombo and M. Nicodemi, *Soft Matter*, 2013, **9**, 8631.
- B.-Y. Ha and Y. Jung, *Soft Matter*, 2015, **11**, 2333–2352.
- Y. Jung and B.-Y. Ha, *Phys. Rev. E: Stat., Nonlinear, Soft Matter Phys.*, 2010, **82**, 051926.
- J. M. Polson and L. G. Montgomery, *J. Chem. Phys.*, 2014, **141**, 164902.
- D. Račko and P. Cifra, *J. Chem. Phys.*, 2013, **138**, 184904.

- 22 Y. Qi, L. Zeng, A. Khorshid, R. J. Hill and W. W. Reisner, *Macromolecules*, 2018, **51**, 617–625.
- 23 V. J. Anderson and H. N. W. Lekkerkerker, *Nature*, 2002, **416**, 811–815.
- 24 M. Dijkstra, J. M. Brader and R. Evans, *J. Phys.: Condens. Matter*, 1999, **11**, 10079–10106.
- 25 G. D'Adamo, A. Pelissetto and C. Pierleoni, *Macromolecules*, 2016, **49**, 5266–5280.
- 26 F. Brochard and P. G. de Gennes, *Europhys. Lett.*, 1986, **1**, 221–224.
- 27 R. A. Omari, A. M. Aneese, C. A. Grabowski and A. Mukhopadhyay, *J. Phys. Chem. B*, 2009, **113**, 8449–8452.
- 28 L.-H. Cai, S. Panyukov and M. Rubinstein, *Macromolecules*, 2015, **48**, 847–862.
- 29 T. Ge, J. T. Kalathi, J. D. Halverson, G. S. Grest and M. Rubinstein, *Macromolecules*, 2017, **50**, 1749–1754.
- 30 R. L. C. Vink, K. Binder and J. Horbach, *Phys. Rev. E: Stat., Nonlinear, Soft Matter Phys.*, 2006, **73**, 056118.
- 31 A. Pérez-Ramírez, S. Figueroa-Gerstenmaier and G. Odriozola, *J. Chem. Phys.*, 2017, **146**, 104903.
- 32 L.-T. Yan, N. Popp, S.-K. Ghosh and A. Böker, *ACS Nano*, 2010, **4**, 913–920.
- 33 L. D. Gelb, K. E. Gubbins, R. Radhakrishnan and M. Sliwinska-Bartkowiak, *Rep. Prog. Phys.*, 1999, **62**, 1573–1659.
- 34 S. Million-Weaver and M. Camps, *Plasmid*, 2014, **75**, 27–36.
- 35 R. Reyes-Lamothe, T. Tran, D. Meas, L. Lee, A. M. Li, D. J. Sherratt and M. E. Tolmasy, *Nucleic Acids Res.*, 2013, **42**, 1042–1051.
- 36 Y. Wang, P. Penkul and J. N. Milstein, *Biophys. J.*, 2016, **111**, 467–479.
- 37 M. J. Shon and A. E. Cohen, *J. Am. Chem. Soc.*, 2012, **134**, 14618–14623.
- 38 S. E. Douglas, T. T. Perkins and S. Chu, *Macromolecules*, 1996, **29**, 1372.
- 39 P.-K. Lin, C.-C. Fu, Y.-L. Chen, Y.-R. Chen, P.-K. Wei, C. H. Kuan and W. S. Fann, *Phys. Rev. E: Stat., Nonlinear, Soft Matter Phys.*, 2007, **76**, 011806.
- 40 D. J. Bonthuis, C. Meyer, D. Stein and C. Dekker, *Phys. Rev. Lett.*, 2008, **101**, 108303.
- 41 N. P. Higgins and A. V. Vologodskii, *Plasmids: Biology and Impact in Biotechnology and Discovery*, American Society of Microbiology, 2015, pp. 105–131.
- 42 Y. L. Lyubchenko and L. S. Shlyakhtenko, *Proc. Natl. Acad. Sci. U. S. A.*, 1997, **94**, 496–501.
- 43 B. Kundukad, J. Yan and P. S. Doyle, *Soft Matter*, 2014, **10**, 9721–9728.
- 44 T. Sakaue, *Macromolecules*, 2007, **40**, 5206–5211.
- 45 M. Doi, *Soft Matter Physics*, Oxford University Press, 2013.
- 46 A. Kusumi, Y. Sako and M. Yamamoto, *Biophys. J.*, 1993, **65**, 2021–2040.
- 47 D. E. Smith, T. T. Perkins and S. Chu, *Macromolecules*, 1996, **29**, 1372–1373.
- 48 E. A. Strychalski, S. L. Levy and H. G. Craighead, *Macromolecules*, 2008, **41**, 7716–7721.
- 49 A. Balducci, P. Mao, J. Han and P. S. Doyle, *Macromolecules*, 2006, **39**, 6273–6281.
- 50 G. Voordouw, Z. Kam, N. Borochov and H. Eisenberg, *Biophys. Chem.*, 1978, **8**, 171–189.
- 51 J. Pelletier, K. Halvorsen, B.-Y. Ha, R. Paparcone, S. J. Sandler, C. L. Woldringh, W. P. Wong and S. Jun, *Proc. Natl. Acad. Sci. U. S. A.*, 2012, **109**, E2649–E2656.
- 52 J. Kim, C. Jeon, H. Jeong, Y. Jung and B.-Y. Ha, *Soft Matter*, 2015, **11**, 1877–1888.
- 53 Y. Chen, W. Yu, J. Wang and K. Luo, *J. Chem. Phys.*, 2015, **143**, 134904.